Nader Pourmahmoud , Amir Hassanzadeh , Seyyed Ehsan Rafiee, Masoud Rahimi
Email: s.e.rafiee@mee.uut.ac.ir

Three-Dimensional Numerical Investigation of Effect of Convergent Nozzles on the Energy Separation in a Vortex Tube

Nader Pourmahmoud *, Amir Hassanzadeh* , Seyyed Ehsan Rafiee°, Masoud Rahimi^

*Department of Mechanical Engineering, Urmia University, Urmia, Iran

°Department of Mechanical Engineering, Kermanshah Branch, Islamic Azad University, Kermanshah, Iran

^ Department of Mechanical Engineering, Urmia University of Technology, Urmia, Iran

ABSTRACT

A computational fluid dynamics (CFD) investigation has been conducted to realize the effect of convergent nozzles on the cooling capacity enhancement of vortex tube. The CFD models have involved turbulent, compressible and axisymmetric swirling flow utilizing the standard k-ε turbulence model. The studied vortex tube has been equipped with the six convergent nozzles. Convergence angle of applied nozzles showed a significant role in achieving to the highest degree of refrigeration, such that the maximum possible amount of cold temperature difference is provided at the angle of 8° (degree respect to nozzle entrance). Therefore, to be presented numerical results include of performance curves, temperature separation rate and particularly swirling flow angular velocity as an important criterion represent a reasonable justification. Finally, obtained results particularly temperature differences are compared with some of the available experimental data which show good agreement.

Keywords: Vortex tube; Divergent nozzles; Numerical simulation; Temperature separation

1. INTRODUCTION

Ranque-Hilsch Vortex Tube (RHVT) is a simple device with no moving parts, which is capable of separating a high-pressure gas flow into two streams of lower pressure flows with different temperatures. As shown schematically in fig. 1, this phenomenon occurs when compressed gas (arbitrary air) flows tangentially into the vortex chamber through the inlet nozzles. The device consists of a simple circular tube, with one or more azimuthally nozzles for flow inlet and two outlets for separated flows exit. High pressure air enters the tube azimuthally and produces a strong vortex flow in the tube. The gas, then, expands gradually through the longitudinal length of tube and achieves a high angular velocity; causing a vortex-type flow. Separating cold and hot streams, by using the principles of the vortex tube can be applied to industrial applications such as cooling equipment in CNC machines, spot cooling, cooling suits, heating processes and etc.

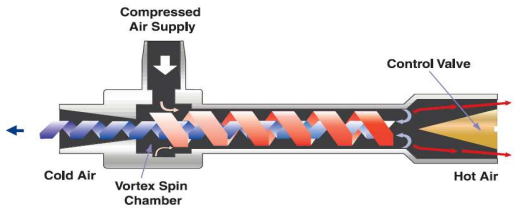

Fig. 1. Schematic drawing of the vortex tube system

The vortex tube is well-suited for these applications because it is simple, compact, light, quiet, and does not use Freon or other refrigerants (CFCs/HCFCs). They are popular for their reliability (no moving parts), lack of maintenance and simple and inexpensive construction. There are two exits on the tube: the hot exit is placed near the outer radius of the tube at the end away from the nozzles, and the cold exit at the center of the tube in the bottom of vortex chambers. Separating of compressed inlet gas into two different temperature streams (cold and hot) is referred as temperature separation effect that reported for the first time by Ranque in 1931 [1]; when he was studying processes in a dust separation cyclone. His design of the vortex tube was later improved by the German physicist Hilsch in 1947 [2], who arranged a diaphragm at the cold exit end of machine. He suggested that angular velocity gradients in the radial direction give rise due to frictional coupling between different layers of the highly rotating flow. Therefore, the transform of energy via shear work would occur from the inner layers to the outer ones. Other investigators have attributed the energy separation to work transfer via compression and expansion, although several variations of this theory are described in the literatures. Similarly, Harnett and Eckert [3] invoked the influence of turbulent eddies and Ahlborn and Gordon [4] described an embedded secondary circulation. Stephan et al. [5] proposed the formation of Gortler vortices on the inside wall of the vortex tube that drive the fluid motion. Kurosaka [6] inferred the temperature separation to be a result of acoustic streaming

effect that transfers energy from the cold core to the hot outer annulus. Gutsol [7] hypothesized the energy separation would be a consequence of micro volumes interactions in the vortex tube. Despite all the proposed theories, none has been able to explain perfectly the temperature separation effect satisfactorily.

Recent efforts have successfully utilized computational fluid dynamics (CFD) modeling to explore the fundamental principles behind the energy separation produced by the vortex tube. Frohlingsdorf et al. [8] modeled the flow within a vortex tube using a CFD solver that included compressible and turbulence effects. The numerical predictions qualitatively predicted the experimental results presented by Bruun [9]. Aljuwayhel et al. [10] employed a fluid dynamics model of the vortex tube to understand the process deriving the temperature separation phenomena. They reported the energy separation exhibited by the vortex tube is due to the work transfer caused by a torque produced by viscous shear acting on a rotating control surface that separates the cold and hot flows. Skye et al. [11] used a model similar to that of Aljuwayhel et al. [10]. They also measured the emitted inlet and outlet temperatures and compared them with the predicted corresponding values of CFD model. Bramo and Pourmahmoud [12] studied numerically the effect of length to diameter ratio (L/D) of tube and the importance of stagnation point occurrence in flow patterns. Pourmahmoud et al. [13] numerically investigated the effect of inlet pressure on the performance of vortex tube.

Recent efforts have successfully utilized computational fluid dynamics (CFD) modeling to explore the fundamental principles behind the energy separation produced by the vortex tube. Frohlingsdorf et al. [8] modeled the flow within a vortex tube using a CFD solver that included compressible and turbulence effects. The numerical predictions qualitatively predicted the experimental results presented by Bruun [9]. Aljuwayhel et al. [10] employed a fluid dynamics model of the vortex tube to understand the process deriving the temperature separation phenomena. They reported the energy separation exhibited by the vortex tube is due to the work transfer caused by a torque produced by viscous shear acting on a rotating control surface that separates the cold and hot flows. Skye et al. [11] used a model similar to that of Aljuwayhel et al. [10]. They also measured the emitted inlet and outlet temperatures and compared them with the predicted corresponding values of CFD model. Bramo and Pourmahmoud [12] studied numerically the effect of length to diameter ratio (L/D) of tube and the importance of stagnation point occurrence in flow patterns. Pourmahmoud et al. [13] numerically investigated the effect of inlet pressure on the performance of vortex tube.

However, among them the nozzle geometrical shape is a specific case because it can significantly enhance the entrance tangential velocity passing through the chamber. The present investigation, therefore, based on the industrial requirements in increasing of vortex tube cooling capacity, would tend to explore the effects of convergent nozzles geometry. Specifically, since fabricating of this type of nozzles on the vortex chamber even in the more number is simple rather than helical or any curved type nozzles; their application seems to be useful from engineering economical point of view.

2. Schematic of the problem geometry

The CFD models of present research are based on the analysis of Skye et al. [11] experimental vortex tube; which basic overall computational assumptions is illustrated in fig. 2. As represented, this system contains six circumferential pressurized gas inlets (injection nozzles), two axial orifices for cold and hot streams and ideal gas which is arbitrary air as working fluid. Since the studied vortex tube equipped with 6 straight nozzles, then the computational domain of generated CFD models are assumed to be a rotational periodic regions. Therefore, only a part of sector is taken for analysis in given cyclic boundary condition; a sector of the flow domain with angle 60° (Akhesmeh et al. [14]).

Papers, including figures and tables, should be limited to about 8 camera ready pages. Please limit your paper by writing concisely, not by reducing the figures to a size at which their labels will be difficult to read.

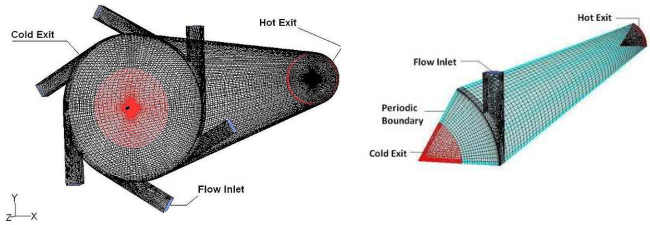

(a) (b)

Figure 2. a) 3D CFD model of vortex tube with six straight nozzles b) A part of sector that is taken for analysis

Details of geometrical dimensions for the Skye's experimental vortex tube are described in table 1. The appropriate boundary conditions are also determined based on the experimental measurements of Skye et al. [11] only for the base model. The static pressure at the cold exit end is set to experimental measurement values, and the static pressure at the hot exit end is adjusted in the way to vary the cold mass fraction. The entrance of injection nozzles is considered as a mass flow inlet, which the specified total mass flow rate and stagnation temperature are maintained to 8.35 gr s^{-1} and 294.2 K, respectively.

Table 1: Geometric summery of CFD models used for vortex tube

Measurement	Skye et al. (2006) experimental vortex tube
Working tube length	106 mm
Working tube diameter	11.4 mm
Nozzle height	0.97 mm
Nozzle width	1.41 mm
Nozzle total inlet area(4_n)	8.2 mm^2
Cold exit diameter	6.2 mm
Hot exit area	95 mm^2

3. GOVERNING EQUATIONS

Since the 1930s, the mechanism of the energy separation inside the RHVT system has puzzled researchers. Even now, there is no clear theory that can explain the phenomenon completely. Nevertheless, significant efforts have been carried out to explore the nature of complex highly rotating flow through vortex tube either experimentally or numerically simultaneously. According to conventional numerical simulation approaches, in the present research modeling of the vortex tube flow field behavior has been analyzed by the

Fluent Code (version: 6.3.26). This computer program allows calculations for compressible fully turbulent flows, which the governing equations (per unit volume) can be solved for general cases. Thus, following of relevant equations in the bellow form introduces continuity, momentums and energy relations, respectively.

$$\frac{\partial}{\partial x_j}(\rho u_j) = 0 \quad (1)$$

$$\frac{\partial}{\partial x_j}(\rho u_i u_j) = -\frac{\partial p}{\partial x_i} + \frac{\partial}{\partial x_j}\left[\mu\left(\frac{\partial u_i}{\partial x_j} + \frac{\partial u_j}{\partial x_i} - \frac{2}{3}\delta_{ij}\frac{\partial u_k}{\partial x_k}\right)\right] + \frac{\partial}{\partial x_j}(-\overline{\rho u_i' u_j'}) \quad (2)$$

$$\frac{\partial}{\partial x_i}\left[u_i \rho\left(h + \frac{1}{2}u_j u_j\right)\right] = \frac{\partial}{\partial x_j}\left[k_{eff}\frac{\partial T}{\partial x_j} + u_i(\tau_{ij})_{eff}\right] \quad (3)$$

$$k_{eff} = K + \frac{c_p \mu_t}{\mathrm{Pr}_t}$$

Since it is assumed the working fluid is an ideal gas, then one can impose the compressibility effect so that:

$$p = \rho RT \quad (4)$$

Flow in the vortex tube is intensively turbulent, therefore steady state assumption together with practical considerations indicate the necessity of utilizing turbulence model. In this way, the standard k-ε turbulence model is applied to the compressible Navier-Stokes equations for numerical analyzing of computational domain. The turbulence kinetic energy, k, and its rate of dissipation, ε are obtained from the following transport equations:

$$\frac{\partial}{\partial t}(\rho k) + \frac{\partial}{\partial x_i}(\rho k u_i) = \frac{\partial}{\partial x_j}\left[(\mu + \frac{\mu_t}{\sigma_k})\frac{\partial k}{\partial x_j}\right] + G_k + G_b - \rho\varepsilon - Y_M \quad (5)$$

$$\frac{\partial}{\partial t}(\rho\varepsilon) + \frac{\partial}{\partial x_i}(\rho\varepsilon u_i) = \frac{\partial}{\partial x_j}\left[(\mu + \frac{\mu_t}{\sigma_\varepsilon})\frac{\partial \varepsilon}{\partial x_j}\right] + C_{1\varepsilon}\frac{\varepsilon}{k}(G_k + C_{3\varepsilon}G_b) - C_{2\varepsilon}\rho\frac{\varepsilon^2}{k} \quad (6)$$

Where, G_k represents the generation of turbulence kinetic energy due to the mean velocity gradients and G_b is the generation of turbulence kinetic energy due to buoyancy which is neglected in this case. Y_M represents the contribution of the fluctuating in compressible turbulence to the overall dissipation rate and $C_{1\varepsilon}$, $C_{2\varepsilon}$ and $C_{3\varepsilon}$ are coefficients. σ_k and σ_ε are the turbulent prandtl numbers for k and ε, respectively. The turbulent viscosity, μ_t ,is computed by combining k and ε as follows:

$$\mu_t = \rho C_\mu \frac{k^2}{\varepsilon} \quad (7)$$

Where, C_μ is a constant. The model constants $C_{1\varepsilon}$, $C_{2\varepsilon}$, C_μ, σ_k and σ_ε have the following default values: $C_{1\varepsilon} = 1.44$, $C_{2\varepsilon} = 1.92$, $C_\mu = 0.09$, $\sigma_k = 1.0$, $\sigma_\varepsilon = 1.3$.

4. Results and discussion

4.1 Validation

As illustrated in figs.3 and 4, the obtained temperature difference at the present analysis for the vortex tube with 6 straight nozzles, were compared with the experimental and computational results of Skye et al. [11]. Both models have obeyed similar geometry and boundary conditions. The Skye et al. [11] CFD model was developed in a two-dimensional form, but the present one is three dimensional. In fig. 4, the ΔTi,h, is predicted by proposed CFD model and is in good agreement with the corresponding experimental values. Prediction of the ΔTi,c is found to be located between the experimental and computational results of Skye et al. [11], which has been shown in fig. 3. The simulated ΔTi,h at both models was close to the experimental results. Though, both models get ΔTi,c lower than the experimental results, the prediction from the present model is found to be closer to the mentioned experiment. In fig. 3 the maximum ΔTi,c is obtained at a cold mass fraction (ε) of about 0.3 through the experiment and CFD simulations. The applied 3D CFD model can produce hot gas temperature of 363.2 K at ε=0.8 and a minimum cold gas temperature of 250.24 K at about 0.3 cold mass fraction.

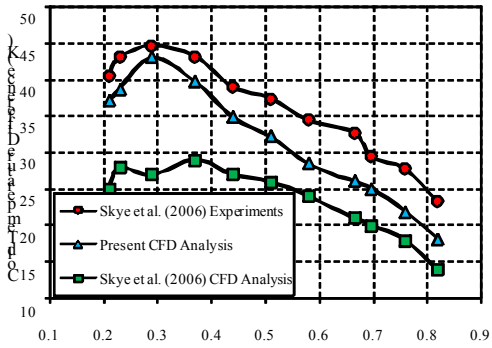

Figure 3. Comparison of cold exit temperature differences with the experimental data

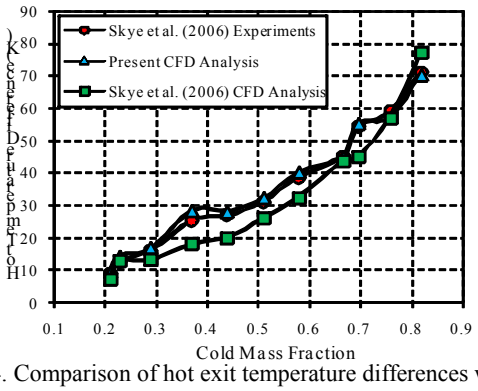

Figure 4. Comparison of hot exit temperature differences with the experimental data

4.2 GRID INDEPENDENCE STUDY

The 3D CFD analysis has been carried out for different average unit cell volumes in vortex tube as a computational domain. This is because of removing probable errors arising due to grid coarseness. Hence, first the grid independence study has been accomplished for ε=0.3. According to presented results in the fig. 3, at this cold mass fraction the vortex tube (with 6 straight nozzles) attains a minimum outlet cold gas temperature. Thus, in the following evaluations we use ε=0.3 as a special value of cold mass fraction. The variation of cold exit temperature difference and maximum swirl (tangential) velocity as the key parameters are shown in figs. 5 and 6 respectively for different unit cell volumes. Not much significant advantage can be seen in reducing of the unit cell volume size below 0.0257 mm^3; which corresponds to 2 87000 cells. The same type of unit cell volume of grids is used to study of the introduced vortex tube with different type of nozzles.

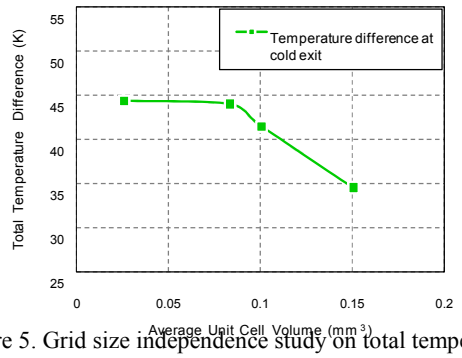

Figure 5. Grid size independence study on total temperature difference at different average unit cell volume

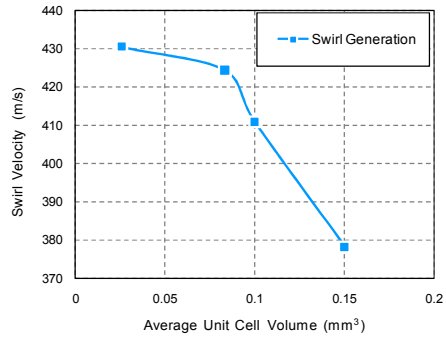

Figure 6. Grid size independence study on maximum swirl velocity at different average unit cell volume

4.3 THE INFLUENCE OF CONVERGENT NOZZLES

In vortex tube, shape type and number of inlet nozzles are quite important. So far, many investigations have been conducted on these parameters in order to achieve the best performance of vortex tube upon minimum cold outlet temperature. Kirmaci and Uluer [15] investigated the vortex tube performance experimentally. They used 2, 3, 4, 5 and 6 numbers of nozzles with air inlet pressures varying from 150 kPa to 700 kPa, and the cold mass fractions of 0.5–0.7. Prabakaran and Vaidyanathan [16] considered the effect of nozzle diameter on energy separation. Shamsoddini and Hossein Nezhad [17] numerically evaluated the effects of nozzles number on the flow and power of cooling of a counter flow vortex tube. They inferred that as the number of nozzles is increased, power of cooling increases significantly while cold outlet temperature decreases moderately. Behera et al. [18] also studied the effect of nozzle shape and number numerically. All of implied investigations reported that the shape of inlet nozzles should be designed such that the flow enters tangentially into vortex tube chamber. Pourmahmoud et al. [19] numerically researched the effect of helical nozzles effect on the performance and cooling capacity of a vortex tube. They [20] also introduced a new parameter named GPL (nozzle inlet gap per length of nozzle) for designing this kind of nozzles. In order to study the influence of convergent inlet nozzles, 6 different convergent angles have been arranged for the vortex tube with fixed geometry; as shown in the fig. 7.
The β implies to angle of convergence and, therefore generated CFD models involve different values for this parameter including 2, 4, 6, 8 and 10°. One can note that the angle of convergence is measured from the entrance of any nozzle, so that the nozzles have the same dimensional geometry.

These results in the terms of temperature differences between hot and cold exits have been represented in figs. 8-10. It can be noted that among the applied convergence angles, the maximum amount of energy separation belongs to angle of 8°, although the amounts of average temperature differences are always smaller than the maximum ones. Hence, it would be preferred to choose this dimension for nozzles as the appropriate geometry, and considered as optimum value of convergence angle. In other words, nozzles

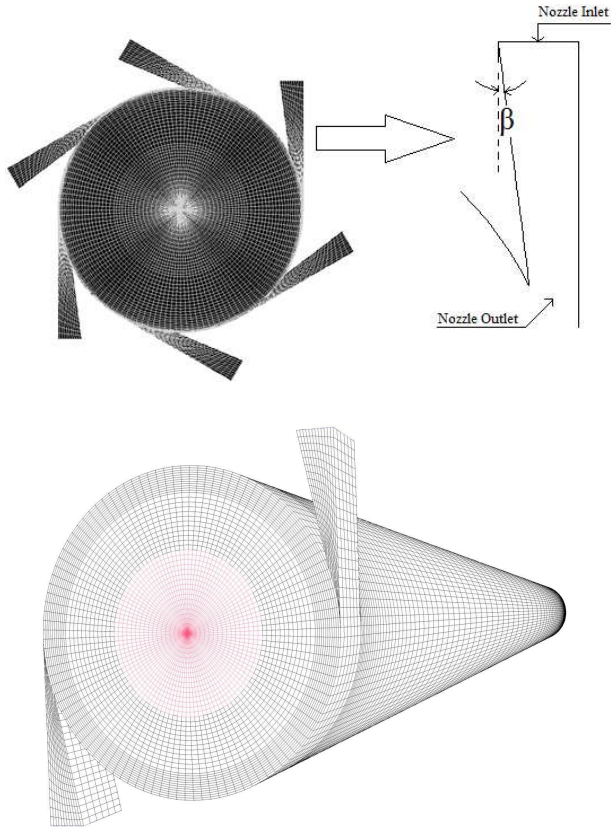

Figure 7. The geometrical shape of convergent inlet nozzles

at these geometry arrangements properly help to form of the highest tangential velocity at the edge of vortex chamber. In respect of varying nozzle angle, radial profiles of axial velocity at different axial locations (z/L = 0.1, 0.4 and 0.7) for a specified cold mass fraction of 0.3 are depicted in fig. 11. The maximum axial velocity for the angle of β=8° (optimum case of nozzles convergence) at axial locations of z/L=0.1, 0.4 and 0.7 was found 108, 67 and 61 m s^{-1}, respectively. In addition, a maximum value of 108 [m s^{-1}] is seen at the tube axis near the inlet zone (z/L=0.1). The corresponding radial velocity profiles for the swirl velocity at z/L=0.1, 0.4 and 0.7 are shown in fig. 12. Comparing the two types of velocity components, thus, it is clear that swirl velocity has the higher value than axial velocity. The radial profile of the swirl velocity indicates a free vortex near the wall and gradually becomes negligibly small at the core, which their physically trend are in good conformity with the observations of Kurosaka [6], Gutsol [7] and Behera et al. [18].

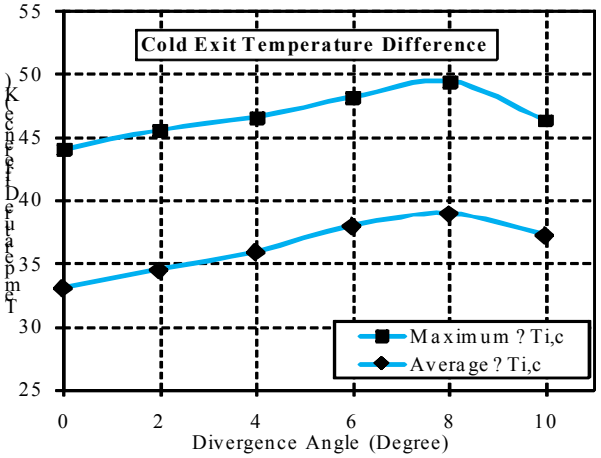

Figure 8. Temperature difference at cold exit for vortex tube with different convergent nozzles

In respect of varying nozzle angle, radial profiles of axial velocity at different axial locations (z/L = 0.1, 0.4 and 0.7) for a specified cold mass fraction of 0.3 are depicted in fig. 11. The maximum axial velocity for the angle of β=8° (optimum case of nozzles convergence) at axial locations of z/L=0.1, 0.4 and 0.7 was found 108, 67 and 61 m s^{-1}, respectively. In addition, a maximum value of 108 [m s^{-1}] is seen at the tube axis near the inlet zone (z/L =0.1).

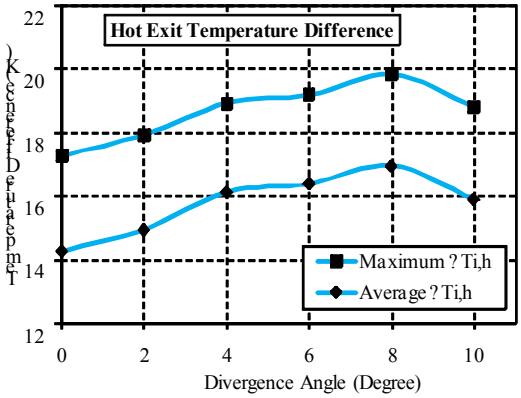

Figure 9. Temperature difference at hot exit for vortex tube with different convergent nozzles

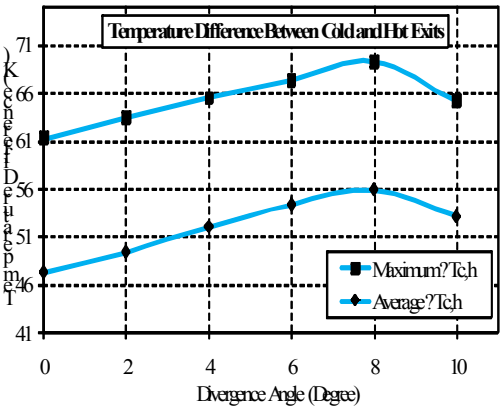

Figure 10. Temperature difference between hot and cold exits for vortex tube with different convergent nozzles

The corresponding radial velocity profiles for the swirl velocity at z/L=0.1, 0.4 and 0.7 are shown in fig. 12. Comparing the two types of velocity components, thus, it is clear that swirl velocity has the higher value than axial velocity. The radial profile of the swirl velocity indicates a free vortex near the wall and gradually becomes negligibly small at the core, which their physically trend are in good conformity with the observations of Kurosaka [6], Gutsol [7] and Behera et al. [18].

Figure 12 shows that in the near of inlet zone (z/L=0.1), and in comparing with other models the highest swirl velocity belongs to model with β=8°. Increasing the distance from inlet zone towards the hot end the swirl velocity magnitude decreases in all models**.** The total temperature variations for vortex tubes equipped with different kinds of convergent nozzles are portrayed in fig. 13. It occurs near the periphery of the tube wall in all of models. Comparing the total temperature and the swirl velocity curves (figs. 12 and 13) shows that there is a correlation between the low temperature zones with negligibly small swirl velocity at the core of rotating flow. The total temperature profiles, also, reveal an increasing of working fluid layers temperature towards the periphery of tube. In fig.13 (a) and (c), the model with β=8° produces both minimum cold and maximum hot exit gas temperatures. The radial variations of the total pressure for different convergence angles are depicted in fig. 14. The most expansion occurs at the nozzles exit end, which causes increasing of injected flow velocity into vortex chamber, and finally working fluid moves as far as hot exit end. Since there are two counter rotating vortices inside tube, the inner rotating flow is formed when a part of flow is returned due to stagnation point. Then, the gas expands again, up to cold outlet; where its pressure drops to atmospheric level. The maximum total pressure appears near the periphery of tube wall in all of simulated CFD models. Comparing the total temperature and the total pressure profiles (figs. 13 and 14) shows the low temperature zone in the core coincides with the low total pressure zone.

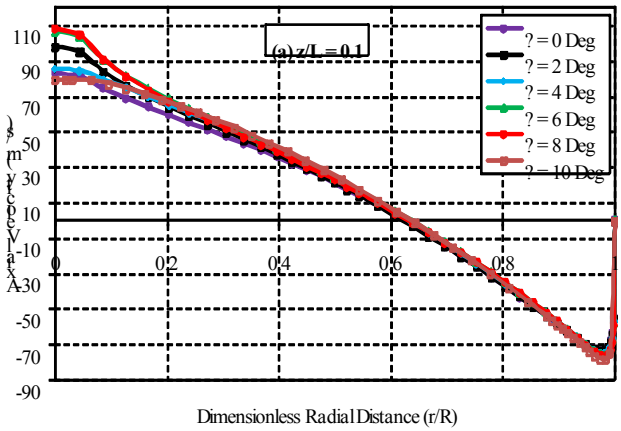

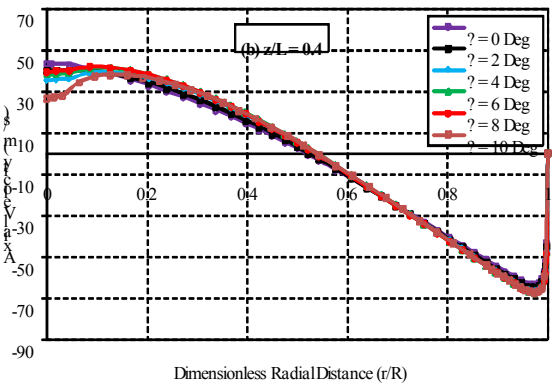

Nader Pourmahmoud , Amir Hassanzadeh , Seyyed Ehsan Rafiee, Masoud Rahimi
Email: s.e.rafiee@mee.uut.ac.ir

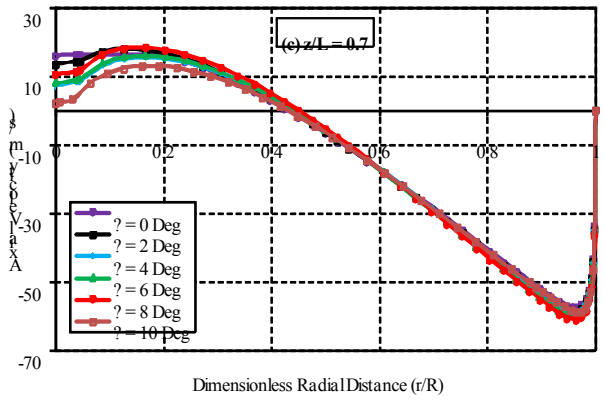

Figure 11. Radial profiles of axial velocity at different axial locations for α=0.3

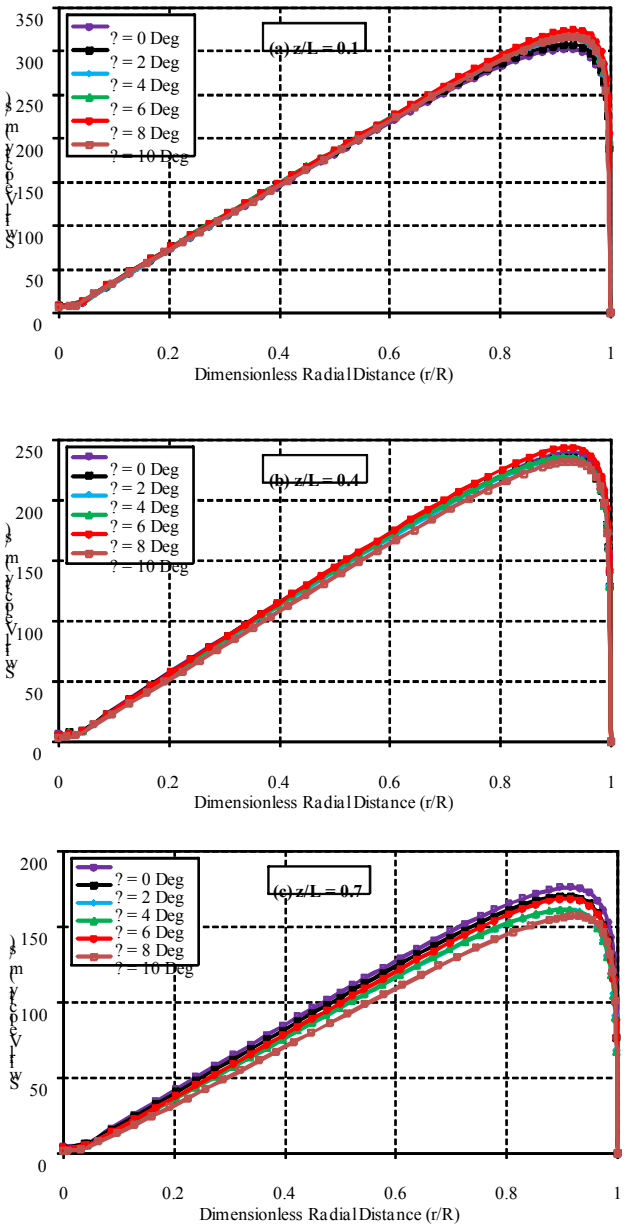

Figure 12. Radial profiles of swirl velocity at different axial locations for α=0.3

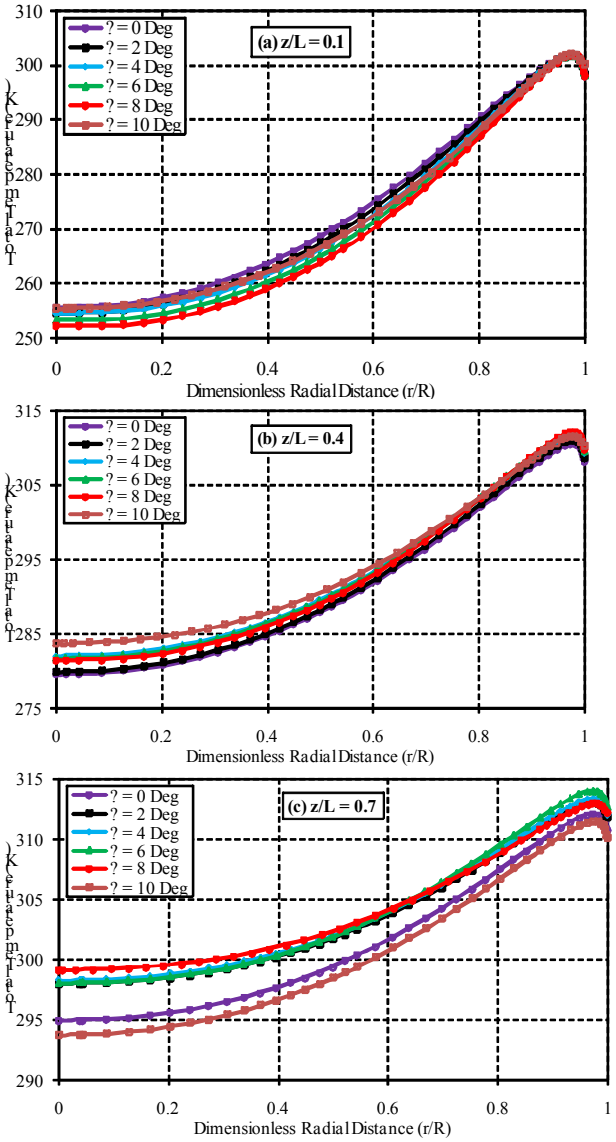

Figure 13. Radial profiles of total temperature at different axial locations for α=0.3

The total pressure profiles (fig.14) show an increase of the pressure values towards the periphery.
The total temperature distribution for optimized angle (β=8°) is displayed in fig. 15. Clearly can be seen that peripheral flow is warm and core flow is cold. Furthermore, increasing of temperature is observed in radial direction.

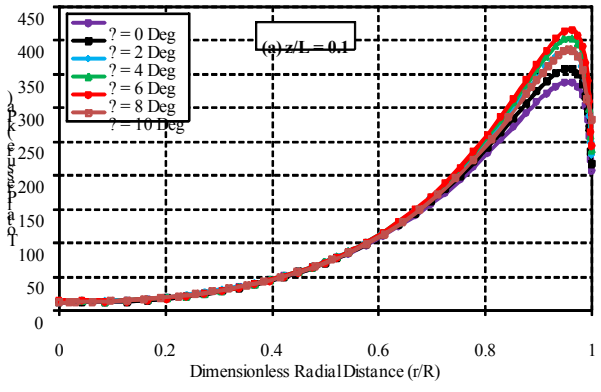

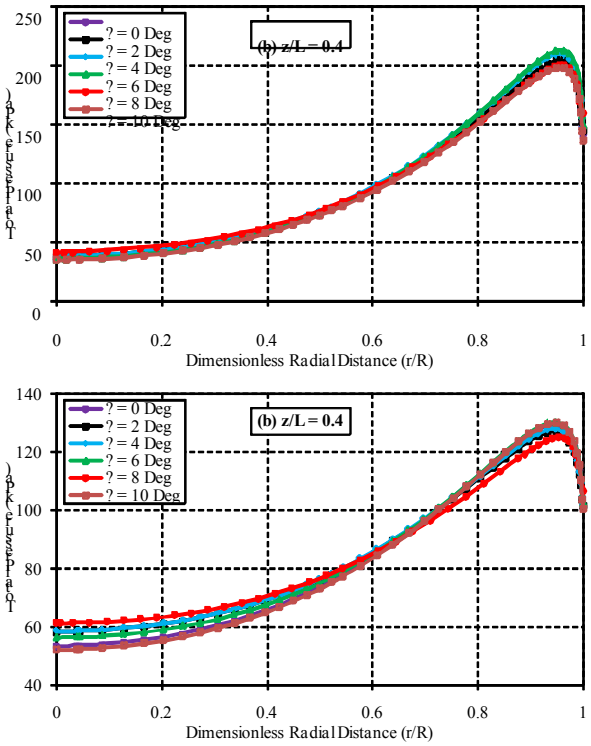

Figure 14. Radial profiles of total pressure at different axial locations for α=0.3

The optimum model of this study, for a cold mass fraction of about 0.3, gives the maximum hot gas temperature of 314.06 K and minimum cold gas temperature of 244.81 K. By comparing these amounts with the CFD model of Skye experiments (maximum hot gas temperature of 311.5 K and minimum cold gas temperature of 250.24 K), one can see the increase of 2.56 K for hot air exit temperature and 5.43 K for cold air exit temperature.

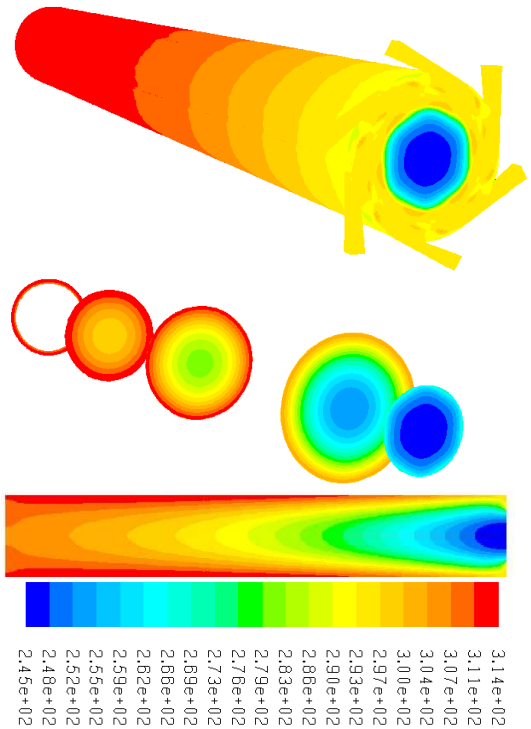

Figure 15. Contours of total temperature for optimum vortex tube, α=0.3

Fig. 16 illustrates the angular velocity profiles (i.e. the rate of flow rotation) as a function of tube radius at different axial locations. Obviously, it is clear that the angular velocity gradually drops in the radial direction, except near the centerline; Of course, in the case of β=8° one can see somewhat difference with the other cases. It is important to note that this becomes at the axial location z/L=0.1, which is a significant location in the vortex tube.

As a comparison the maximum swirl velocity, when a vortex tube equipped by 6 straight nozzles is reached to 428 m s^{-1} (Bramo and Pourmahmoud [12]) at the vortex tube; while in the present case of studied nozzles the flow angular velocity finally approaches to 436 m s^{-1}. Thus an improvement in the swirl velocity can be seen.

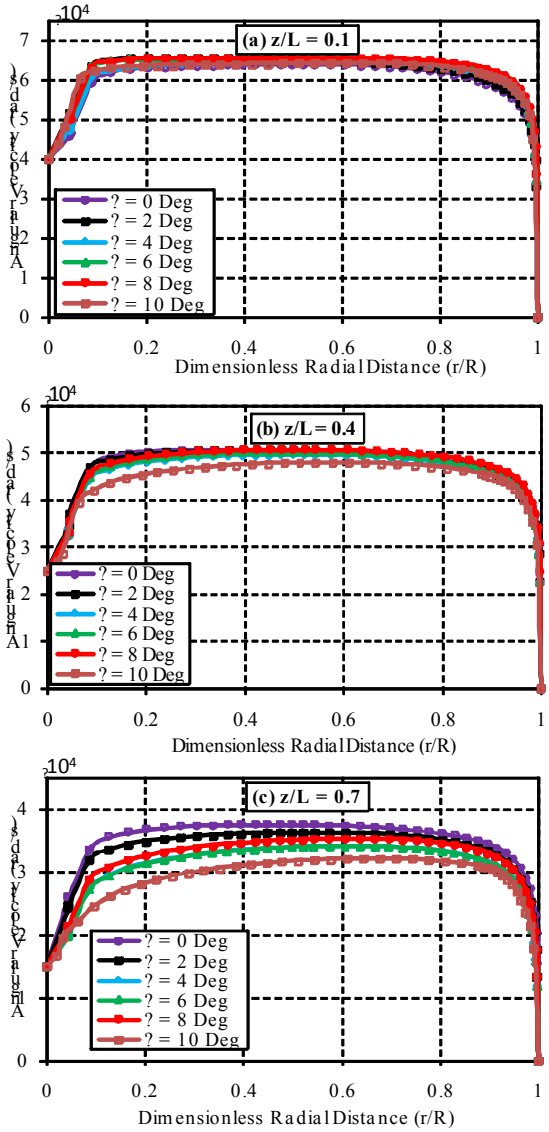

Figure 16. Radial profiles of angular velocity at different axial locations, α=0.3

4. CONCLUSION

A three dimensional computation has been carried out to investigate convergent nozzles effect on the improving of vortex tube cooling capacity. The generated CFD models

analyzed a complex compressible and turbulent fluid flow throughout a vortex tube as computational domain, together with assuming of an axisymmetric flow field. In addition, for exhibiting of turbulent flow structure inside the thermo dynamical system, the standard k-ε turbulence model is utilized. The main aim of research is based on establishing of convergent nozzles geometrical arrangement such that the highest swirl velocity is formed in the vortex chamber. Hence, numerical simulations were conducted due to many various convergence angles for nozzles. The temperature separation either cold or hot exit temperature differences as judgment criteria revealed an optimum angle of convergence; 8°. This angle which is measured respect to the nozzles entrance, would lead to form of the highest tangential velocity at the edge of vortex chamber. Both cooling and heating temperature curves are derived for a specific cold mass fraction equal to 0.3, which is a reasonable value to give the appropriate temperature separation condition in this study. Consequently, by fixing the number of convergent nozzles (6 numbers) at their final geometry, the obtained numerical results comparison were performed with the case of straight nozzles. As a comparison the maximum swirl velocity, when a vortex tube equipped by 6 convergent nozzles is seen to increase. Finally some of evaluated results especially temperature differences are compared with the available experimental data and good agreement yielded.

5. REFERENCES

1. G.J. Ranque, Experiments on expansion in a vortex with simultaneous exhaust of hot air and cold air, *J. Phys. Radium* (Paris), vol. 4, pp. 112-115, 1933.
2. R. Hilsch, The use of expansion of gases in a centrifugal field as a cooling process, *Rev. Sci. Instrum*, vol. 18, pp. 108-113, 1947.
3. J. Harnett, E. Eckert, Experimental study of the velocity and temperature distribution in a high velocity vortex-type flow, *Trans. ASME* , vol.79, pp. 751-758, 1957.
4. B.K. Ahlborn, J.M. Gordon, The vortex tube as a classic thermodynamic refrigeration cycle, *J. Appl. Phys,* vol. 88 (6), pp. 3645-3653, 2000.
5. K. Stephan, S. Lin, M. Durst, F. Huang, D. Seher, An investigation of energy separation in a vortex tube, *Int. J. Heat Mass Transfer,* vol. 26 (3), pp. 341–348, 1983.
6. M. Kurosaka, Acoustic streaming in swirling flows, *J. Fluid Mech*, vol. 124, pp. 139-172, 1982.
7. A.F. Gutsol, The Ranque effect. *Phys. Uspekhi*, vol. 40, pp. 639-658, 1997.
8. W. Frohlingsdorf, H. Unger, Numerical investigations of the compressible flow and the energy separation in the Ranque-Hilsch vortex tube, *Int. J. Heat Mass Transfer*, vol. 42, pp. 415-422, 1999.
9. H.H. Bruun, Experimental investigation of the energy separation in vortex tubes, *J. Mech. Eng. Sci*, vol. 11, pp. 567-582, 1969.
10. N.F. Aljuwayhel, G.F. Nellis, S.A. Klein, Parametric and internal study of the vortex tube using a CFD model, *Int. J. Refrigeration*, vol. 28, pp. 442-450, 2005.
11. H.M. Skye, G.F. Nellis, S.A. Klein, Comparison of CFD analysis to empirical data in a commercial vortex tube, *Int. J. Refrigeration*, vol. 29, pp. 71-80, 2006.
12. A.R. Bramo, N. Pourmahmoud, CFD simulation of length to diameter ratio effect on the energy separation in a vortex tube, *Therm. Sci*. vol.15(3), 833-848, 2011.
13. N. Pourmahmoud, , A. Hassan Zadeh, O. Moutaby, A.R. Bramo, Numerical investigation of operating pressure effects on the performance of a vortex tube, *Therm. Sci*. doi:10.2298/TSCI110907030P.
14. S. Akhesmeh, N. Pourmahmoud, H. Sedgi, Numerical study of the temperature separation in the Ranque-Hilsch vortex tube, *Am. J. Eng. Appl. Sci*, vol. 3, pp. 181-187, 2008.
15. V. Kirmaci, O. Uluer, An experimental investigation of the cold mass fraction, nozzle number and inlet pressure effects on performance of counter flow vortex tube. *J. Heat Transfer-Trans. ASME*, vol.8 (131), pp. 081701-081709, 2009.
16. J. Prabakaran, S. Vaidyanathan, Effect of diameter of orifice and nozzle on the performance of counter flow vortex tube, *Int. J. Eng. Sci. Tech*, vol. 2 (4), pp. 704-707. 2010.
17. R. Shamsoddini, A. Hossein Nezhad, Numerical analysis of the effects of nozzles number on the flow and power of cooling of a vortex tube, *Int. J. Refrigeration,* vol. 33, pp. 774-782, 2010.
18. U. Behera, P.J. Paul, S. Kasthurirengen, R. Karunanithi, S. N. Ram, K. Dinesh, S. Jacob, CFD analysis and experimental investigations towards optimizing the parameters of Ranque– Hilsch vortex tube, *Int. J. Heat Mass Transfer*, vol. 48, pp. 1961–1973, 2005.
19. N. Pourmahmoud, A. Hassan Zadeh, O. Moutaby, A.R. Bramo, Computational fluid dynamics analysis of helical nozzles effects on the energy separation in a vortex tube. *Therm. Sci*, vol.16 (1), pp. 151–166, 2012.
20. N. Pourmahmoud, A. Hassan Zadeh, O. Moutaby, Numerical analysis of the effect of helical nozzles gap on the cooling capacity of Ranque–Hilsch vortex tube, *Int. J. Refrigeration*, vol. 35 (5), pp. 1473-1483, 2012.

Nomenclature

D	Diameter of vortex tube [mm]
k	Turbulence kinetic energy [$m^2 s^{-2}$]
L	Length of vortex tube [mm]
r	Radial distance measured from the centerline of tube [mm]
R	Radius vortex tube
T	Temperature [K]
z	Axial length from nozzle cross section [mm]

Greek Symbols

α	Cold mass fraction
β	Convergence angle of nozzles
ε	Turbulence dissipation rate [$m^2 s^{-3}$]
$\Delta T_{c,h}$	Temperature difference between cold and hot ends [K]
$\Delta T_{i,c}$	Temperature difference between inlet and cold ends [K]
$\Delta T_{i,h}$	Temperature difference between hot end and inlet [K]
ρ	Density [kg m^{-3}]
μ	Dynamic viscosity [kg $m^{-1} s^{-1}$]
μ_t	Turbulent viscosity [kg $m^{-1} s^{-1}$]
τ_{ij}	Stress tensor components